SEMARAK ILMU PUBLISHING

Journal of Advanced Research in Fluid Mechanics and Thermal Sciences

Journal homepage:
https://semarakilmu.com.my/journals/index.php/fluid_mechanics_thermal_sciences/index
ISSN: 2289-7879

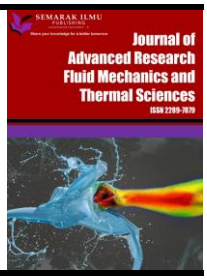

Vibration-Induced Flow and Streaming in Oscillatory Flow of Thermoacoustics

Azman Hafiidz Aji[1], Fatimah Al Zahrah Mohd Saat[1,2,*], Fadhilah Shikh Anuar[1,2], Patcharin Saechan[3]

[1] Fakulti Teknologi dan Kejuruteraan Mekanikal (FTKM), Universiti Teknikal Malaysia Melaka (UTeM), Hang Tuah Jaya 76100 Durian Tunggal, Melaka, Malaysia
[2] Green and Efficient Energy Technology (GrEET), Centre for Advanced Research on Energy (CARE), Universiti Teknikal Malaysia Melaka (UTeM), Hang Tuah Jaya, 76100 Durian Tunggal, Melaka, Malaysia
[3] Department of Mechanical & Aerospace Engineering, Faculty of Engineering, King Mongkut's University of Technology North Bangkok, 1518 Pracharat 1 Rd., Bangsue, Bangkok, 10800, Thailand

ARTICLE INFO

Article history:
Received 23 October 2023
Received in revised form 20 February 2024
Accepted 3 March 2024
Available online 30 March 2024

Keywords:
Thermoacoustics; oscillatory flow; flow streaming; stack; vibration

ABSTRACT

Induced acoustic streaming flow in thermoacoustic systems occurs due to acoustic vibrations, causing changes to the mean flow in the systems. This phenomenon creates a tendency to generate net fluid flow that can cause energy change within certain areas inside the system. However, the effects of the entire system's vibrations on the flow streaming are not yet fully understood, yet it is important for a more effective operation. This study experimentally investigated the flow streaming resulting from vibration in a standing-wave thermoacoustic test rig with a flow frequency of 23.6 Hz. The existence of flow streaming due to vibration which was not counted in the theoretical formula is shown and indicated by experimental values. The result shows that there is a correlation between the amplitude of the drive ratio (DR) and the velocity of the oscillation of the flow. Upon examining both the theoretical and the practical evidence, it becomes clear that there exists a marginal flow velocity in directions other than the main flow due to the vibration of resonator's wall as measured at the intake and outflow areas of the stack. This marginal flow velocity amplifies as the drive ratio of flow increases and it may potentially explain the observed difference between measured flow amplitude and the theoretical value.

1. Introduction

Nowadays, a trend in the extraction of waste heat energy derives from many types of sources such as solar energy, geothermal power and industrial operation has become a spotlight in research and innovation works [1-4]. The current waste heat technology includes absorption systems, mechanically driven heat exchangers, and organic Rankine cycles are among the available energy conversion systems [5-7]. In general, thermoacoustics principles can be used in to design and develop energy conversion devices, such as generators and refrigerators [8,9]. In thermoacoustics, the fluid exhibits flow characteristics that are influenced by specific acoustic wave conditions. Understanding

* *Corresponding author.*
E-mail address: fatimah@utem.edu.my

https://doi.org/10.37934/arfmts.115.2.112

the fluid dynamics of flow in these systems is difficult because it has a significant impact on the overall efficacy of the system. This is primarily due to the complex nature of acoustic waves and the unique characteristics of passage through objects or structures [10].

Currently, the scope of thermoacoustics also presents opportunities for enhancing energy conversion and has made a significant advancement in the field of thermoacoustic research. These result to a system with better efficiency, a distinct advantage over the conventional thermoacoustic systems. The improvements made in the thermoacoustic system can be seen in the context of improved performance in low temperature at different system operation, higher pressure amplitudes, and innovative designs [11]. Consequently, these systems hold promise for a variety of applications, including low-grade heat recovery and residential air conditioning systems. It is important to acknowledge that thermoacoustic systems utilize non-traditional working substances due to the unique advantages as compared to the conventional thermoacoustic systems. The benefits are evidenced in enhancing the efficiency and demonstrated better capacity for utilization in the recovery of low-grade heat [12]. Normally, the established fluid dynamics of flow in multiple conventional systems served as a point of reference for predicting fluid dynamics behaviors. The flow pattern shows that the flux does indeed exhibit disparities as reported by Saat and Jaworski [13]. The flow pattern within thermoacoustics differs from that of normal flow due to the cyclic nature of the flow, as was also demonstrated by previous research [14]. The generation of acoustic waves occurs at specific frequencies within the field of thermoacoustics, resulting in the unavoidable vibration of the system. Despite this, the influence of the entire system's vibration on thermoacoustic flow remains largely unexplored.

On the other hand, previous study by Kayes and Rahman [15] attained an ideal configuration of the stack inside parametric domain. Furthermore, the study offered an understanding of the fundamental principles that elucidate the observed phenomena. In the ideal configuration, there is a reduction of 58% in the generation of higher harmonics, while the maximum acoustic output is attained at a comparatively low starting temperature of 13°C. The thermoacoustic environment is less understood in terms of its behaviour due to the change of flow conditions. This was previously indicated and studied by Saat *et al.,* [16] through an experimental work on the oscillatory flow in thermoacoustic environment. Through the study, two different flow frequencies of 14.2 Hz and 23.6Hz inside a standing wave thermoacoustic rig have been determined.

Meanwhile, Aliev *et al.,* [17] examined the velocity profiles of internally imposed plate vibrations and their corresponding sound pressure levels in the far field across several resonant modes. The study focused on examining the processes to determine the change of vibrational modes for compressed thermoacoustic sources by manipulating the size and thickness of the vibrating plates, as well as the depth of the cavity. The study found that a reduction in the thickness of a plate is associated with a drop in its resonance frequency and an increase in the amplitude of its vibrations within the given material environment. The substantial cyclic variation in cavity volume, which arises in the core of a confined plate's boundary, is also improved. Simultaneously, the edges of the plate experience a displacement that counters the overall change in volume.

The one-directional flow condition and the bi-directional flow condition in several thermoacoustic energy systems are also studied by Hasbullah *et al.,* [18] by examining the characteristics of the flow and the operational mechanism of the systems The study found that there are significant differences between the behaviors of unidirectional and bidirectional flow situations in relation to the trends of velocity and temperature variations among the findings from the experimental works.

Another research work conducted by Saechan and Dhuchakallaya [19] studied a typical thermoacoustic system that comprised of an open structure known as a stack. The stack is enclosed

within a resonator with a closed boundary. In Figure 1, it can be shown that the magnitude of the peak-to-peak shift results in the displacement of a singular gas parcel towards the left, indicating movement towards a region characterized by greater pressure. This displacement is accompanied by a reduction in size due to diabatic compression. At this stage, the gas parcel exhibits elevated levels of both pressure and temperature. Subsequently, the transfer of thermal energy occurs from the heated heat exchanger to the plate of the stack, with the pressure being constant.

The volume of the gas decreases due to the alteration in temperature. Subsequently, the gas parcel undergoes oscillatory motion in the right direction, moving towards a region of lower pressure, as a diabatic expansion occurs. As the pressure of the gas parcel decreases, a corresponding decrease in its temperature is also seen. Ultimately, the temperature of the gas parcel decreases to a level lower than that of the stack plate. In the condition when the pressure remains constant, the thermal energy originating from the stack plate will transfer to the gas parcel. The increase in the quantity of the cooling gas is attributed to thermal expansion.

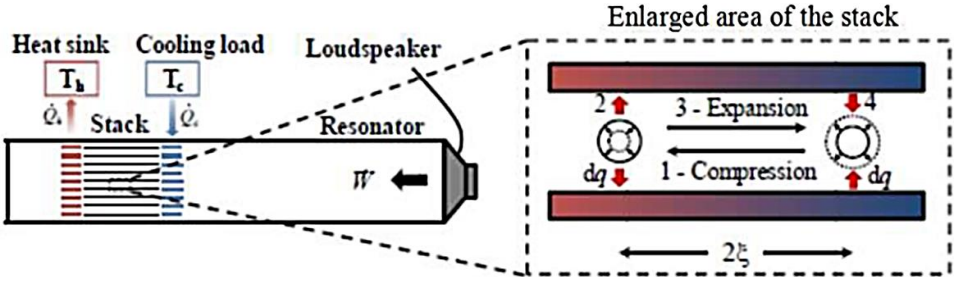

Fig. 1. The working principal of standing wave thermoacoustic [19]

As an addition, the heat cycle occurs between the gas parcels inside the flow and the solid surfaces of the stack. This is the location where the gas packets undergo compression followed by expansion. The oscillatory pattern of flow is observed and replicate to perpetuate the cyclic process. Each individual gas packet facilitates the transfer of a little amount of heat from the colder region on the left to the hotter region on the right. This phenomenon results in a heat transfer process known as a heat pumping effect. The phenomenon referred to as the "thermoacoustic effect" is the designated term for this thermal process [19].

Conversely, if a substantial temperature disparity exists between the upper and lower regions of the stack, the resultant phenomenon of a sound wave will be triggered, hence facilitating the generation of electricity. This implies that the thermoacoustic concept can be employed to facilitate thermodynamic processes that have the potential to achieve cooling or power generation.

Flow streaming in thermoacoustic systems can arises from the presence of acoustic vibrations, which can lead to temperature changes and subsequently generate a net fluid flow within a limited area. The observed phenomenon may be attributed to the interaction between acoustic waves and the fluid in the system. This effect is frequently observed in various devices such as thermoacoustic engines and refrigerators. This study presents the empirical findings of potential flow streaming because of vibration effects on the structure of the thermoacoustic test rig. However, this can be improved by acquiring knowledge about the additional flow streams and factors that contribute to discrepancies between experimental evidence and theoretical predictions of thermoacoustic energy conversion. In this study, the vibration effect to the flow streaming is investigated using an experimental work. The aimed is to emphasize on the flow streaming condition caused by the vibration effect.

2. Methodology

2.1 Experimental Test-Rig Setup

The aim of this research work was achieved by conducting experimental work. The schematic diagram of the experimental test rig is as shown in Figure 2. The experimental test rig consists of three main components which are a loudspeaker, a resonator and porous structure known as a stack. The loudspeaker functions as an acoustic driver that supplies and generates soundwave inside the resonator. The soundwave travels along the resonator through the stack which is located inside the resonator. The resonator is built up as a straight duct based on the quarter wavelength setup as was reported in Allafi and Saat [20].

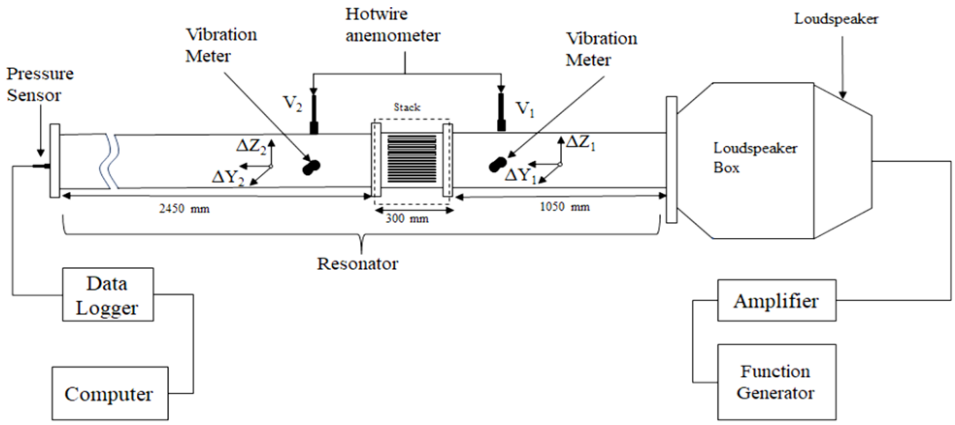

Fig. 2. Schematic diagram of the experimental setup

The resonator that is connected to the loudspeaker box is as given in Figure 3(a) and Figure 3(b), respectively. The resonator is fabricated using hollow square cross-sectional duct of 146 mm x 146 mm with wall thickness of 3 mm. The resonator is 3.8 m long.

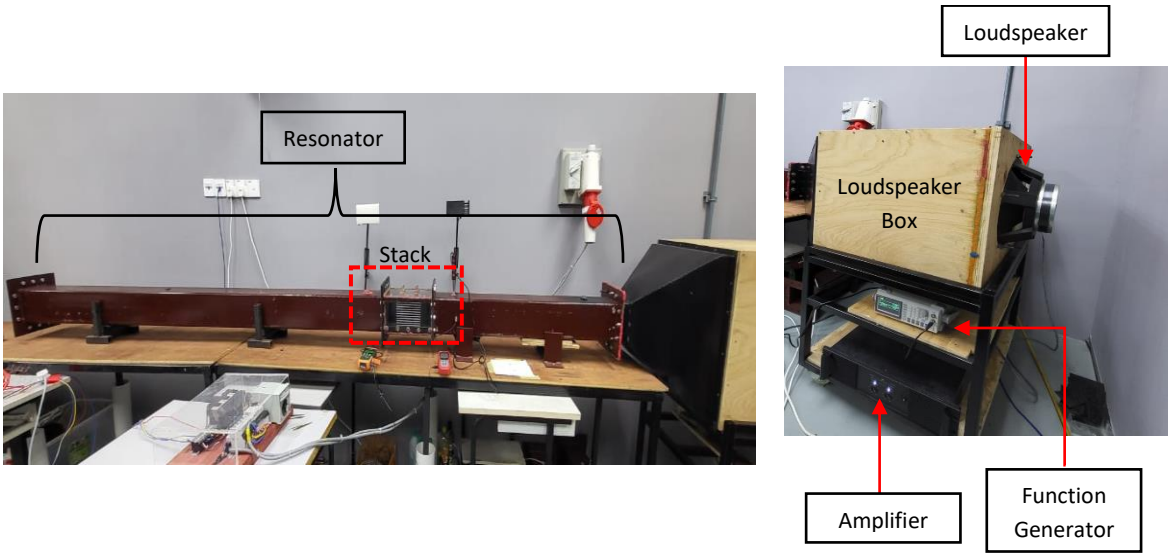

(a) (b)

Fig. 3. The experimental setup: (a) Resonator and Stack, (b) Loudspeaker to drive the flow

The acoustic standing wave that was generated between the resonator and the loudspeaker is a quarter wavelength type where pressure is calculated to be maximum at the closed end of the resonator where the pressure sensor was placed. The quarter wavelength is described

mathematically as $\lambda/4$ where the wavelength, λ is equal to the fraction of the speed of sound with the flow frequency, $\lambda = c/f$. The constant value of 346 m/s was used as the speed of sound as the experiment was conducted in a room temperature. The previous study conducted by Saat *et al.,* [16] was referred to for the resonance frequency of 23.6 Hz and 3.8 m length of resonator. Figure 4 shows the resonance frequency value that was identified to be at 23.6 Hz.

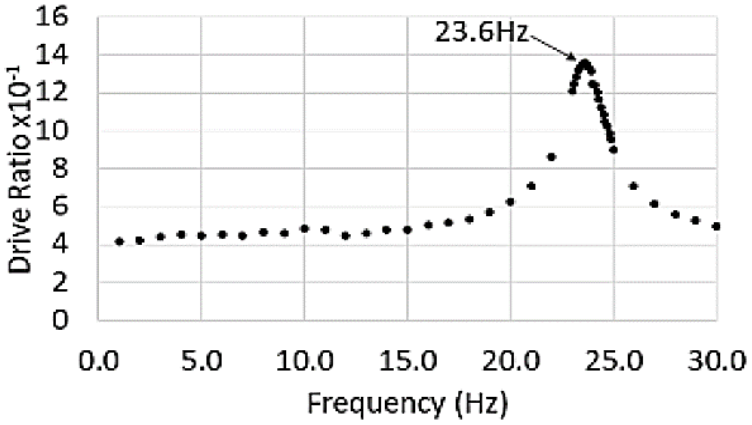

Fig. 4. Resonance frequency for the 3.8 m long resonator [16]

The stack plate was fabricated using aluminum as the material, which has a thermal conductivity of 237 W/m.K and a specific heat capacity of 903 J/kg.K. The plate is arranged and placed inside the hollow cross-section column. The arrangement of plates within the resonator is as shown in Figure 5 The details about the stack and its dimensions are as tabulated in Table 1.

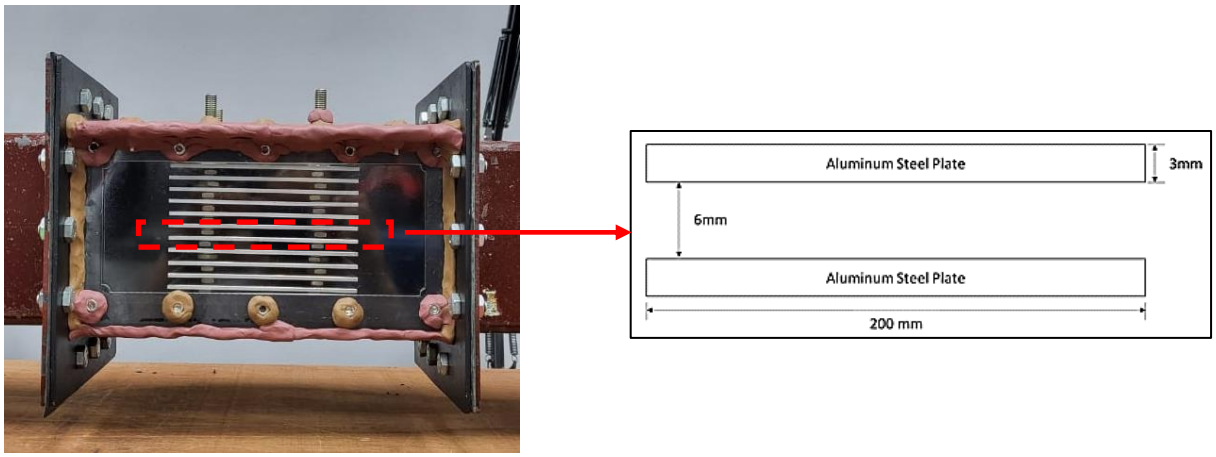

Fig. 5. The parallel plate assembly of the stack inside the test section area of the resonator

Table 1
Test rig configuration

Parameter	Value
Number of parallel plates	16
Thickness of plate (mm)	3
Gap between plates(mm)	6
Length of plate (mm)	200

As was shown in Figure 3(b), the 18-inch loudspeaker model PD1860 was used to generate an acoustic wave that was controlled by the amplifier model FLP-MT 21005 and the signal was given by a function generator model AFG 21005 which was connected to an amplifier. In this experiment, the

output from the function generator to the loudspeaker was set to 23.6 Hz with peak-to-peak Voltage (V_{pp}) ranging at 0.05 V to 0.5 V, with 0.05 increments for each value.

At the upstream and downstream locations of the stack, as shown in Figure 6, a hotwire anemometer model ST-732 was utilized to measure the velocity amplitude of the flow, *V*. The displacement of the resonator's body due to vibration was measured along the *z*- and *y*-axes using a model Extech SDL800 accelerometer. The instrument is positioned 270 mm upstream and downstream of the test rig's center.

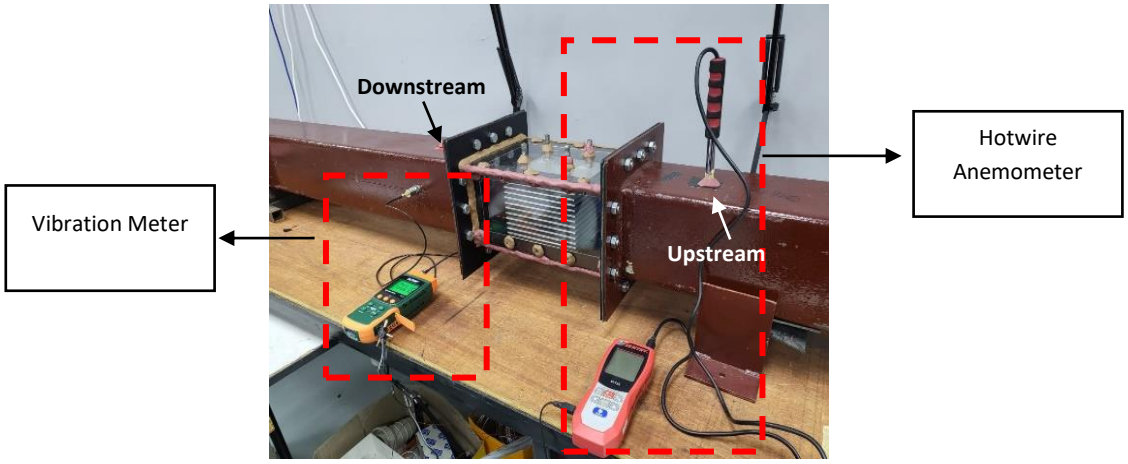

Fig. 6. Experimental setup of measuring equipment near the stack

At the end of the resonator, the dynamic piezoresistive pressure sensor as shown in Figure 7(a) was used to acquire the amplitude of the pressure at the location of pressure antinode, P_a, which represents the maximal pressure of the flow. The pressure sensor's input and output wires are connected to a 12 DC power supply and a Dataq DI-718B datalogger as shown in Figure 7(b).

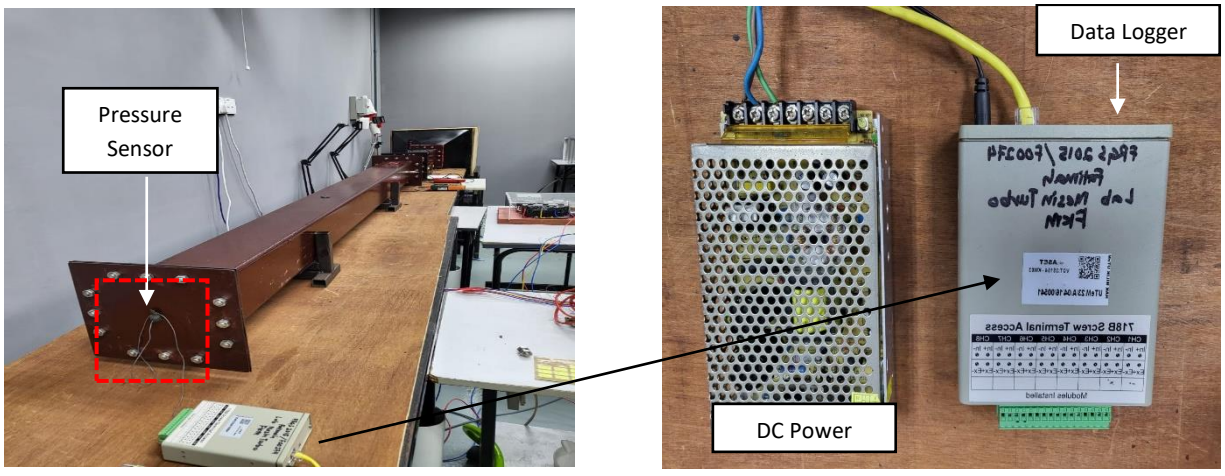

(a) (b)

Fig. 7. (a) Location of the pressure sensor and (b) the direct current (DC) power supply and data logger connections for the pressure sensor's input and output wires

The DC power supply supplied the power to turn on the sensor while the data logger helps collecting the data with the use of WinDaq software that was installed in a computer. The data is read from datalogger using the WinDaq Data Acquisition Software. The uncertainties of instruments are as stated in Table 2.

Table 2
List of devices with the uncertainty value

Instrument	Uncertainty
Loudspeaker	Sensitivity (1w-1m): 95dB
	Frequency range: 30Hz-2kHz
Function Generator	Frequency range: 0.1 ~5MHz
Amplifier	Frequency response: 20Hz – 20kHz±1dB
Pressure sensor	Range: 0-2psiq
	Positive sensitivity: 100+55/-25 mV/psi
Hotwire anemometer	Air velocity: 0-40 ± (0.03) m/s
	Air Flow: 1.8m3/min ± 3% of reading
Vibration meter	Displacement: 0.003 – 1.999mm ± (5% +2d)

The drive ratio (DR), which represents the magnitude of the standing wave, is a significant component within the thermoacoustic framework, characterized by a dimensionless quantity. The drive ratio refers to the ratio between the sound pressure at the pressure antinode, denoted as P_a, and the average mean pressure, denoted as P_m. The pressure antinode location is a specific location within the resonator where the pressure exhibits its maximum intensity. According to the preliminary investigations prior to this study, the location of the pressure antinode is identified as the hard end of the quarter wavelength resonator where pressure sensor could be fitted to monitor the flow amplitude [18,20]. The mean pressure indicates the magnitude of the average air pressure contained within the resonator. For a system that operates at atmospheric pressure, the mean pressure is atmospheric pressure. The gaseous medium employed in this study is air, which is modelled as an ideal gas characterized by an average pressure of 100 N/m^2 and an average temperature of 300 K.

The experimental data consists of the acoustic pressure of the flow at the position of the pressure antinode, P_a expressed in Pascal (Pa), and the velocity of the flow at the upstream and downstream positions, denoted as V_1 and V_2 respectively, measured in meter per second (m/s).

Then, the body's displacement along the *y*- and *z*-axes of the resonator, measured at the upstream and downstream positions of the stack, given in millimeters (mm) are determined. The body's displacement signifies the vibration that has the potential to induce supplementary flow in directions apart from the primary flow direction. Eq. (1) is employed to compute the induced component of flow velocity, $V_{y,z}$, resulting from the displacement of the body, with the aim of estimating the influence of vibration on the flow. The displacement, denoted as Δ_y and Δ_z, was measured utilizing a vibration meter, whereas the flow frequency, represented as *f*, was determined to be 23.6 Hz.

$$V_{y,z} = \Delta_{y,z}(2\pi f) \tag{1}$$

The experimental technique is repeated three times for repeatability test. Eq. (2) and Eq. (3) are employed for the purpose of ascertaining the computations pertaining to uncertainty. The formula represented by Eq. (2) is used to calculate the mean value, indicated as $\overline{x}$, of a dataset. This value is generally known as the average value. The variable "*n*" represents the number of duplicated measurements. The determination of experimental error entails the use of the standard deviation, represented as *σ*, as presented in Eq. (3).

$$\overline{x} = \frac{1}{n}\sum_{i=1}^{n} x_i \text{ where i} = 1,2,3 \ldots . \text{n} \tag{2}$$

$$\sigma = \sqrt{\frac{\sum(x_i - \overline{x})^2}{n-1}} \tag{3}$$

3. Results

The graphical representation in Figure 8 illustrates the investigation of the correlation between the drive ratio variant and the velocity of flow that was observed at a particular location positioned 270 mm from the center of the stack. This analysis involves a comparison between the measured velocity and the computationally computed velocity using the inlet boundary condition of the computational domain as was reported by Allafi and Saat [20] for the flow frequency of 23.6 Hz. Meanwhile, the drive ratio presents a ratio of the sound pressure at the pressure antinode and the mean pressure of the operation. Both variables demonstrate a discernible augmentation in velocity, which can be mathematically expressed by a polynomial function. The finding suggests the existence of acoustic flow within the resonator, wherein the magnitude of the flow intensifies with higher driving ratios. The extent to which the findings obtained from prior research align with those of the present study can be debated considering the notion of comparability. This finding suggests the presence of a positive relationship between the drive ratio and the flow velocity, indicating that an increase in the drive ratio leads to a matching increase in the flow velocity. The graph illustrating the increased experimental velocity displays a notable discrepancy, which can be attributed to several causes and uncertainties inherent in the testing procedure.

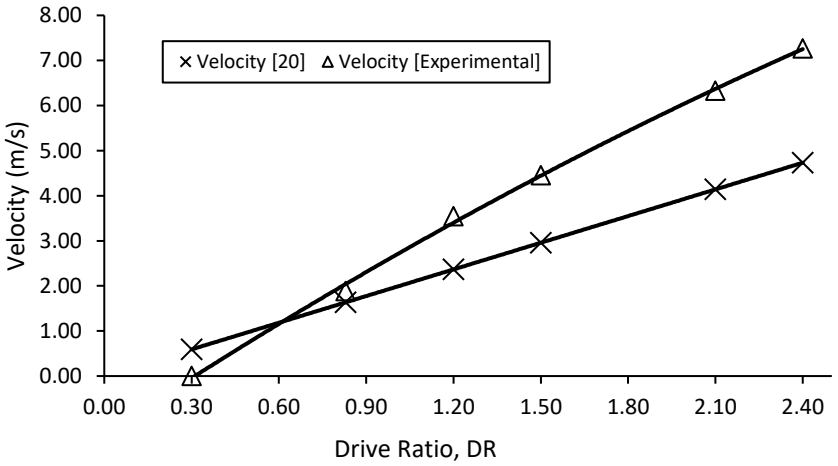

Fig. 8. Comparison between the experimentally measured and the CFD values of velocity amplitude against the Drive Ratio [20]

Figure 9 illustrates the measured velocity of the fluid flow as the drive ratio, DR is incrementally increased, and the accompanying data is presented alongside the theoretical calculation [21]. The theoretical velocity, *V*, is calculated based on Eq. (4):

$$V = \left[\frac{P_a}{\rho.c}\sin(kx)\right]\cos(\omega t) \tag{4}$$

where the terms P_a, k, ρ, c, ω, x, t , correspond to the pressure antinode, the wave number, the density of the working fluid, the speed of sound for air, angular frequency, the position of axial point from the pressure antinode, and time, respectively. The wave number, *k*, can be calculated form Eq. (5) where *f* is the frequency of 23.6 Hz.

$$k = \frac{2\pi f}{c} \tag{5}$$

Similar pattern as in Figure 8 is observed for the results shown in Figure 9. The observed experimental data exhibits a departure from the expected theoretical values, with the magnitude of this deviation increasing as the amplitude of the flow is heightened. It is interesting to note that both the computational fluid dynamics (CFD) data of Allafi and Saat [20] is almost similar to the theoretical values while experimental measurement shows higher values. The projected outcome is predicted to be caused by the impact of the induced flow coming from vibration, which leads to the creation of additional streaming in directions that are not aligned with the axial flow direction. The theoretical framework of linear theory neglected to consider this specific influence. Similarly, the nonlinear effect of flow streaming due to vibration may not be well captured in the two-dimensional CFD model of Allafi and Saat [20]. The disparity between experiment and theory become more significant as drive ratio increases, indicating that the streaming impact is bigger when thermoacoustic's flow amplitude is larger.

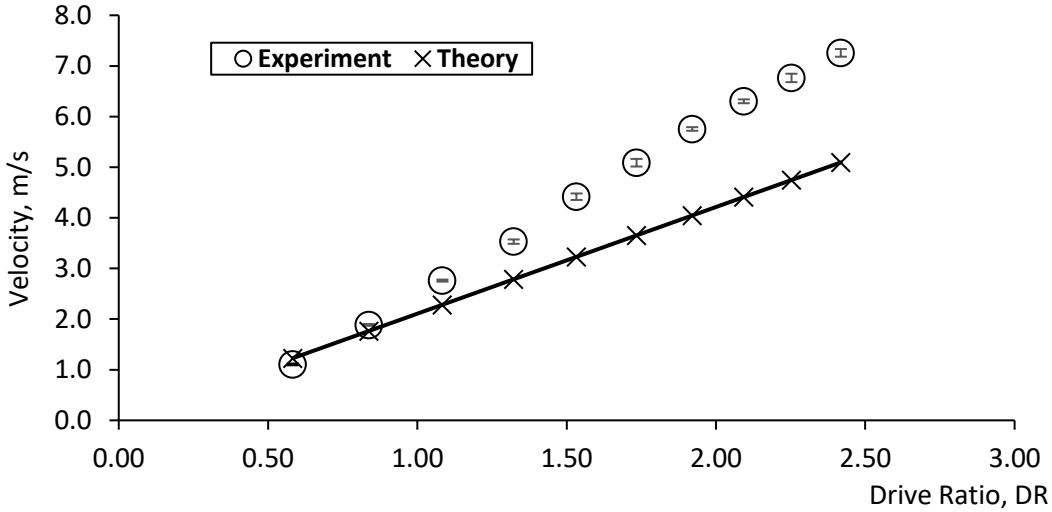

Fig. 9. Experimental and theoretical changes of velocity amplitude of flow with drive ratio

Table 3 presents the measured velocity values for the *y*- and *z*-axes that were acquired from the vibration meter, together with the corresponding values computed using Eq. (1). The subscripts 1, and 2 for V_z and V_y refer to the two different locations of measurement. The locations were as indicated by the vibration meter points in Figure 2. The data suggests that the magnitude of the displacement $\Delta_z$is larger than the magnitude of the displacement Δ_y. This means that the vertical vibration of the resonator is larger than that of the transverse direction. Hence, the vertical component of velocity vector for air flow inside the resonator may contributes as interference (i.e., streaming) to the main flow of the wave. The highest recorded velocity is for Δ_z= 9.984x10^{-3} m/s, which is in comparison to a velocity of 1.997x10^{-3} m/s along the *y*-axes (confer Figure 2 for the illustration of direction of flow). The velocity demonstrates a significant increase, particularly in relation to the displacement along the *z*-axes, which can potentially influence the amplitude of the axial flow or the main flow in thermoacoustics.

Table 3
Velocity different between *y*- and *z*-axes

DR	Vz1 (x10-3m/s)	Vz2 (x10-3m/s)	Vy1 (x10-3m/s)	Vy2 (x10-3m/s)
0.30	0.395	0.395	0.395	0.395
0.55	1.038	1.087	0.445	0.395
0.83	2.215	2.669	0.445	0.445
1.00	3.312	3.213	0.692	0.544
1.20	4.300	4.201	0.939	0.791
1.50	5.289	5.140	1.285	0.939
1.70	6.376	5.981	1.285	0.939
1.90	7.414	6.920	1.631	1.582
2.10	8.205	7.958	1.928	1.730
2.25	9.095	8.600	1.928	1.779
2.40	9.984	9.540	1.977	1.878

The velocity component obtained from the displacement measurement is illustrated in Figure 10. The velocity resulting from body's displacements at *y*-and *z*-axes, represented as $\Delta_{y,z}$ is in accordance with the experimental schematic model as previously illustrated in Figure 2. The graph demonstrates that the magnitude of the velocity in the *z*-axis, $V\mathrm{z}_1$ and $V\mathrm{z}_2$ is larger than that in the *y*-axis. Although the size of this value is relatively minuscule, it's impact could be amplified when it is transferred to the air particles and this will influence the difference in flow amplitude between theoretical predictions and experimental findings, as illustrated in Figure 9.

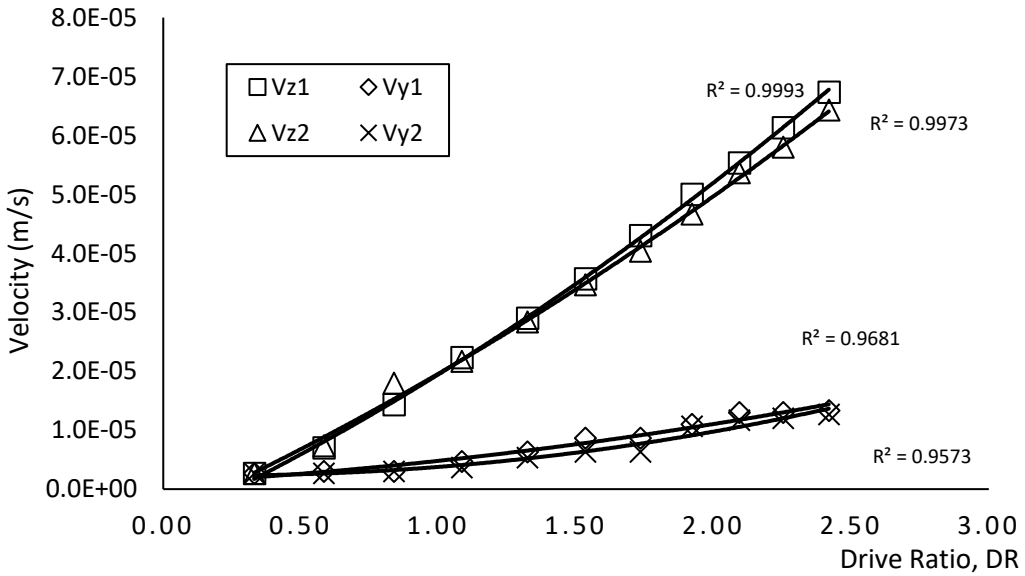

Fig. 10. Velocity from the displacement of Δz and Δy

4. Conclusions

This paper reported the examination of the flow streaming phenomenon that was caused by vibration in the field of thermoacoustics. A positive relation can be seen between the amplitude of the drive ratio (DR) and the velocity amplitude of the oscillatory flow. Through the analysis of theoretical and empirical evidence, it becomes apparent that the marginal flow velocity due to vibration of the wall that is occurring at the intake and outflow of the stack can be potentially accounted for the observed disparity of the mean velocity of the flow between the experiment and the computational flow model. Nevertheless, further investigation is recommended to investigate

the influence of flow streaming to the fluid dynamics within thermoacoustic devices, with the aim of enhancing the existing system's design and operation.

Acknowledgement
The initial part of this work was accepted and presented in ICE-SEAM 2023. The authors would like to thank Universiti Teknikal Malaysia Melaka (UTeM) for providing the research facilities. This research work was ongoing research as part of the works funded by Ministry of Higher Education Malaysia under FRGS/1/2023/TK08/UTEM/02/1.

References

[1] Hassan, Zulkurnain, Mohd Suffian Misaran, Nancy Julius Siambun, Ag Sufiyan Abd Hamid, and Mohd Amran Madlan. "Feasibility of using Solar PV Waste Heat to Regenerate Liquid Desiccant in Solar Liquid Desiccant Air Conditioning System." *Journal of Advanced Research in Experimental Fluid Mechanics and Heat Transfer* 2, no. 1 (2020): 10-16.

[2] Pelda, Johannes, Friederike Stelter, and Stefan Holler. "Potential of integrating industrial waste heat and solar thermal energy into district heating networks in Germany." *Energy* 203 (2020): 117812. https://doi.org/10.1016/j.energy.2020.117812

[3] Emadi, Mohammad Ali, Nazanin Chitgar, Oyeniyi A. Oyewunmi, and Christos N. Markides. "Working-fluid selection and thermoeconomic optimisation of a combined cycle cogeneration dual-loop organic Rankine cycle (ORC) system for solid oxide fuel cell (SOFC) waste-heat recovery." *Applied Energy* 261 (2020): 114384. https://doi.org/10.1016/j.apenergy.2019.114384

[4] Delpech, Bertrand, Massimo Milani, Luca Montorsi, Davide Boscardin, Amisha Chauhan, Sulaiman Almahmoud, Brian Axcell, and Hussam Jouhara. "Energy efficiency enhancement and waste heat recovery in industrial processes by means of the heat pipe technology: Case of the ceramic industry." *Energy* 158 (2018): 656-665. https://doi.org/10.1016/j.energy.2018.06.041

[5] Xu, Z. Y., H. C. Mao, D. S. Liu, and R. Z. Wang. "Waste heat recovery of power plant with large scale serial absorption heat pumps." *Energy* 165 (2018): 1097-1105. https://doi.org/10.1016/j.energy.2018.10.052

[6] Brückner, Sarah, Selina Liu, Laia Miró, Michael Radspieler, Luisa F. Cabeza, and Eberhard Lävemann. "Industrial waste heat recovery technologies: An economic analysis of heat transformation technologies." *Applied Energy* 151 (2015): 157-167. https://doi.org/10.1016/j.apenergy.2015.01.147

[7] Tchanche, Bertrand F., Gr Lambrinos, Antonios Frangoudakis, and George Papadakis. "Low-grade heat conversion into power using organic Rankine cycles-A review of various applications." *Renewable and Sustainable Energy Reviews* 15, no. 8 (2011): 3963-3979. https://doi.org/10.1016/j.rser.2011.07.024

[8] Timmer, Michael A. G., Kees de Blok, and Theo H. van der Meer. "Review on the conversion of thermoacoustic power into electricity." *The Journal of the Acoustical Society of America* 143, no. 2 (2018): 841-857. https://doi.org/10.1121/1.5023395

[9] Sharify, Esmatullah Maiwand, and Shinya Hasegawa. "Traveling-wave thermoacoustic refrigerator driven by a multistage traveling-wave thermoacoustic engine." *Applied Thermal Engineering* 113 (2017): 791-795. https://doi.org/10.1016/j.applthermaleng.2016.11.021

[10] Allafi, Waleed Almukhtar, Fatimah Al Zahrah Mohd Saat, and Xiaoan Mao. "Fluid dynamics of oscillatory flow across parallel-plates in standing-wave thermoacoustic system with two different operation frequencies." *Engineering Science and Technology, an International Journal* 24, no. 1 (2021): 41-49. https://doi.org/10.1016/j.jestch.2020.12.008

[11] Xiao, Lei, Kaiqi Luo, Zhanghua Wu, Jiaxin Chi, Jingyuan Xu, Limin Zhang, Jianying Hu, and Ercang Luo. "A highly efficient heat-driven thermoacoustic cooling system." *Cell Reports Physical Science* (2024). https://doi.org/10.1016/j.energy.2024.130610

[12] Huang, Jiale, Rui Yang, Yupeng Yang, Qiang Zhou, and Ercang Luo. "Generalized thermoacoustic heat engines with unconventional working substances: A review." *Applied Energy* 347 (2023): 121447. https://doi.org/10.1016/j.apenergy.2023.121447

[13] Saat, Fatimah A. Z. Mohd, and Artur J. Jaworski. "Numerical predictions of early stage turbulence in oscillatory flow across parallel-plate heat exchangers of a thermoacoustic system." *Applied Sciences* 7, no. 7 (2017): 673. https://doi.org/10.3390/app7070673

[14] Mustaffa, Siti Hajar Adni, Fatimah Al Zahrah Mohd Saat, and Ernie Mattokit. "Turbulent Vortex Shedding across Internal Structure in Thermoacoustic Oscillatory Flow." *Journal of Advanced Research in Fluid Mechanics and Thermal Sciences* 46, no. 1 (2018): 175-184.

[15] Kayes, Md Imrul, and Md Ashiqur Rahman. "Experimental investigation of a modified parallel stack for wet thermoacoustic engine to improve performance and suppress harmonics." *Applied Acoustics* 212 (2023): 109569. https://doi.org/10.1016/j.apacoust.2023.109569
[16] Saat, Fatimah Al Zahrah Mohd, Dahlia Johari, and Ernie Mattokit. "DeltaE modelling and experimental study of a standing wave thermoacoustic test rig." *Journal of Advanced Research in Fluid Mechanics and Thermal Sciences* 60, no. 2 (2019): 155-165.
[17] Aliev, Ali E., David H. Mueller, Kylie N. Tacker, Nathanael K. Mayo, John B. Blottman, Shashank Priya, and Ray H. Baughman. "Improved thermoacoustic sound projectors by vibration mode modification." *Journal of Sound and Vibration* 524 (2022): 116753. https://doi.org/10.1016/j.jsv.2022.116753
[18] Hasbullah, Nurjannah, Fatimah Al Zahrah Mohd Saat, Fadhilah Shikh Anuar, Mohamad Firdaus Sukri, Mohd Zaid Akop, and Zainuddin Abdul Manan. "Experimental Study on The Performance of One-Directional and Bi-Directional Flow Conditions Across In-Line Tube Banks Heat Exchanger." *Journal of Advanced Research in Fluid Mechanics and Thermal Sciences* 96, no. 2 (2022): 74-87. https://doi.org/10.37934/arfmts.96.2.7487
[19] Saechan, Patcharin, and Isares Dhuchakallaya. "A Study of standing-wave thermoacoustic refrigerator." *International Journal of Physical and Mathematical Sciences* 9, no. 12 (2015): 2100-2105.
[20] Allafi, Waleed Almukhtar, and Fatimah Al Zahrah Mohd Saat. "Entrance and exit effects on oscillatory flow within parallel-plates in standing-wave thermoacoustic system with two different operating frequencies." *Journal of King Saud University-Engineering Sciences* 34, no. 5 (2022): 350-360. https://doi.org/10.1016/j.jksues.2020.12.008
[21] Smith, Walter Fox. *Waves and oscillations: a prelude to quantum mechanics*. Oxford University Press, 2010.